Journal of Photochemistry and Photobiology A: Chemistry 337 (2017) 207–215

Contents lists available at ScienceDirect

Journal of Photochemistry and Photobiology A: Chemistry

journal homepage: www.elsevier.com/locate/jphotochem

Systematic investigation of the excited-state properties of anthracene-dicarboxylic acids

Jennifer M. Rowe, Jennifer M. Hay, William A. Maza, Robert C. Chapleski Jr, Erin Soderstrom, Diego Troya, Amanda J. Morris*

Department of Chemistry, Virginia Polytechnic Institute and State University, Blacksburg, VA, 24061, United States

ARTICLE INFO

Article history:
Received 22 September 2016
Received in revised form 16 November 2016
Accepted 23 December 2016
Available online 24 December 2016

Keywords:
Anthracene
Photoluminescence
DFT calculations

ABSTRACT

We report the photophysical properties of three anthracene-dicarboxylic acids – 1,4-anthracene dicarboxylic acid (1,4-ADCA), 2,6-anthracene dicarboxylic acid (2,6-ADCA) and 9,10-anthracene dicarboxylic acid (9,10-ADCA) – in a series of polar aprotic solvents using steady-state absorption spectroscopy, steady-state emission spectroscopy and time-correlated single photon counting emission lifetime spectroscopy. The addition of carboxylic acid functional groups on the anthracene ring perturbs the electronic transitions oriented along the longitudinal and transverse axes to varying degrees, resulting in differences in the photophysical properties. The three anthracene derivatives exhibit very different excited-state properties in basic solution compared to acidic and neutral solutions. Density functional theory (DFT) calculations reveal that the lowest-energy ground-state structures of both 2,6-ADCA and 1,4-ADCA have dihedral angles between the carboxylic acids and aromatic planes of $\theta = 0°$. For 9,10-ADCA, the same dihedral angle increases to $\theta = 56.6°$. Time-dependent DFT calculations suggest that the carboxyl groups of 1,4-ADCA and 2,6-ADCA remain coplanar with the anthracene ring system in the excited state. In contrast, the calculations reveal significant changes between the ground and excited geometries for 9,10-ADCA as the dihedrals decrease from 56.6° to 27.7° in the first excited state, and puckering of the anthracene moiety of 9,10-ADCA is observed.

1. Introduction

Organic photoactive molecules are of interest due to the tunability and environmental susceptibility of their excited-state properties, which affords a range of optoelectronic applications including organic light-emitting diodes (OLEDs), photovoltaic cells, organic field effect transistors, and fluorescent sensing elements [1–4]. Anthracene is a polyaromatic hydrocarbon whose excited-state properties have been extensively studied [5]. Due to its unique ground and excited-state properties, anthracene and its derivatives are often incorporated into devices such as OLEDs and organic semiconductor materials for numerous applications [6–9]. However, in order to rationally tailor anthracene derivatives for a given application, an understanding of the effects of microenvironment and functionalization on the photophysical properties is essential.

The steady-state absorption and emission spectra of anthracene in THF are shown in Fig. 1. The absorption spectrum of anthracene has two sets of bands in the 220 nm–280 nm and 290 nm–400 nm ranges, corresponding to three different $\pi \rightarrow \pi^*$ transitions. The absorption observed in each region displays vibronic structure and corresponds to one of two transition moments oriented along the molecular axes. The transition dipole of the high-energy transition centered around 256 nm, corresponding to a $^1A \rightarrow {}^1B_b$ transition (Platt notation) [10], is polarized along the longitudinal axis. The low-energy transition centered around 386 nm, corresponding to a $^1A \rightarrow {}^1L_a$ transition, is polarized along the transverse short axis, as illustrated in Fig. 1 [5,11,12]. Another longitudinally polarized transition of $^1A \rightarrow {}^1L_b$ character is also present; however, the oscillator strength of this transition is weak and is obscured by the much more intense $^1A \rightarrow {}^1L_a$ transition band. The mirror-image relationship observed between the $^1A \rightarrow {}^1L_a$ absorption bands and the $^1L_a \rightarrow {}^1A$ emission band is indicative of a negligible change in the nuclear coordinates between the ^1A ground state and ^1L_a excited state from which the emission originates [11,13]. Thus, according to the Frank-Condon principle, the geometry of the excited state of anthracene is similar to that of the ground state.

The positions of both the steady-state absorption and emission maxima of anthracene are independent of solvent polarity or

* Corresponding author.
E-mail address: ajmorris@vt.edu (A.J. Morris).

http://dx.doi.org/10.1016/j.jphotochem.2016.12.021
1010-6030/

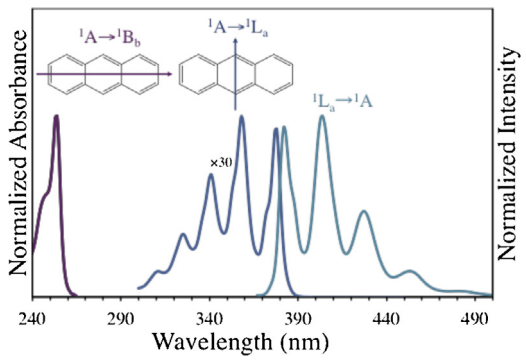

Fig. 1. Absorbance spectrum of anthracene in THF showing the $\pi \rightarrow \pi^*$ transitions with dipole moments oriented along the longitudinal axis ($^1A \rightarrow {}^1B_b$, purple) and across the short axis ($^1A \rightarrow {}^1L_a$, dark blue) of anthracene and emission spectrum arising from the $^1L_a \rightarrow {}^1A$ transition (light blue). (For interpretation of the references to colour in this figure legend, the reader is referred to the web version of this article.)

hydrogen bonding at room temperature [14]. Likewise, the fluorescence quantum yield (Φ_f) and fluorescence lifetime (τ_f) of anthracene are insensitive to changes in solvation environment [15,16]. For example, the fluorescence lifetimes measured in benzene, cyclohexane and ethanol are 4.29 ns, 5.24 ns, and 5.1 ns, respectively, and the quantum yield of fluorescence is between 0.27 and 0.36 in the same solvents [17–20].

The excited-state behavior of a carboxylic acid functionalized anthracene, 9-anthracenecarboxylic acid (9-ACA), has been the topic of a number of reports [21–27]. Changes in the emission spectra of 9-ACA have been argued to arise from acid-base equilibrium, solvent- and concentration-dependent dimerization and formation of higher-order aggregates, as well as structural reorganization of the carboxylic acid relative to the anthracene ring in the excited state [22,24,26]. In order to contribute to this discussion, we prepared a series of anthracene derivatives functionalized symmetrically with carboxylic acids; namely 2,6-anthracenedicarboxylic acid (2,6-ADCA), 1,4-anthracenedicarboxylic acid (1,4-ADCA), and 9,10-anthracenedicarboxylic acid (9,10-ADCA). We characterize the effect of functionalization on the energetics of the ground and excited states of anthracene using steady-state absorption and emission spectroscopies, emission lifetime measurements, density functional theory (DFT) and time-dependent DFT (TDDFT) calculations. The results are interpreted in light of structural/conformational differences between the ground and excited states of each anthracene derivative.

2. Materials and methods

2.1. Materials

2,6-anthracenedicarboxylic acid (2,6-ADCA) [28,29], 1,4-anthracenedicarboxylic acid (1,4-ADCA) [30,31], and 9,10-anthracenedicarboxylic acid (9,10-ADCA) [32] were synthesized following previously reported procedures with minimal modifications and characterized by 1H NMR spectroscopy (Figs. S16–S18) [28–32]. All other chemicals and solvents including anthracene (>99%), KOH (85%), NH_4OH (25–30%), acetic acid (reagent grade > 99%), dimethylformamide (HPLC grade > 99%), dimethylacetamide (spectrophotometric grade > 99%), tetrahydrofuran (ACS grade > 99%), ethyl acetate (HPLC grade > 99.9%), acetone (HPLC grade > 99.5%), and butanone (ACS grade > 99%) were used as received without further purification from Alfa Aesar, Fisher Scientific, or Sigma-Aldrich.

2.2. Steady-state absorption spectroscopy

The steady-state absorption spectra of the ADCA derivatives were obtained using an Agilent Technologies 8453 UV–vis diode array spectrophotometer (1 nm resolution) where the spectra were recorded with samples prepared in a 1-cm quartz cuvette. To determine the extinction coefficients of each compound, three solutions of known concentration ($\sim 5 \times 10^{-5}$ M) were prepared separately, and then each was diluted three times. The UV–vis absorbance of each solution was measured, and the absorbance at a fixed wavelength was plotted vs. concentration. The extinction coefficient was determined by averaging the slopes of the lines-of-best-fit obtained from each of the three plots.

2.3. Steady-state emission spectroscopy and time-resolved emission lifetimes

All samples were prepared at concentrations below 10 μM to reduce aggregation effects and purged with argon before measurements were performed. Time-resolved fluorescence lifetimes were obtained via the time-correlated single photon counting technique (TCSPC) with a modified QuantaMaster Model QM-200-4E emission spectrophotometer from Photon Technology, Inc. (PTI) equipped with a 350 nm LED and a Becker & Hickl GmbH PMH-100 PMT detector with time resolution of < 220 ps full width at half maximum (FWHM) [33]. Florescence lifetime decays were deconvoluted from the time-dependent florescence signal and the instrument response function using the fluorescence decay analysis software, DecayFit, available online (Fluortools, www.fluortools.com, Figs. S13–S15).

Quantum yields of fluorescence and steady-state emission spectra of the ADCA compounds were measured in ethyl acetate, tetrahydrofuran (THF), butanone, acetone, dimethylacetamide (DMA), dimethylformamide (DMF), acidic (acetic acid) DMF and basic (NaOH) DMF. The steady-state emission spectra were obtained using the same QuantaMaster Model QM-200-4E where the sample compartment was replaced with an integrating sphere (PTI). The excitation light source was a 75 W Xe arc lamp (Newport). The detector was a thermoelectrically cooled Hamamatsu 1527 photomultiplier tube (PMT). All measurements were performed in triplicate using three separately prepared solutions of ADCA in each solvent with absorbance values of ~ 0.08–0.09 at the excitation wavelength. Low temperature emission spectra (Fig. S7) were obtained from THF glass solutions immersed in a liquid N_2 filled finger Dewar flask (77 K).

Theoretical calculations: All electronic structure calculations were carried out in the gas phase with the Gaussian 09 suite of programs [34]. The DFT calculations presented in this work were carried out at the B3LYP/6-31G* level [35–38]. Sample calculations using the M06 density functional [39], and the larger 6-311G* basis set [40] were used to corroborate key results at the B3LYP/6-31G* level. Ground-state potential-energy contours correspond to relaxed scans in which the relevant dihedral angles between the carboxylic acid groups and the anthracene moiety are allowed to vary at 15° steps while the rest of the coordinates are optimized. Potential-energy contours for the carboxylic acids in the lowest energy singlet excited state were obtained using time-dependent B3LYP/6-31G* calculations [41–43], directly using the geometries obtained from ground-state dihedral scans. Lowest-energy structures from both the ground and excited state contours were fully optimized, and vibrational analysis was performed to confirm that these structures correspond with minima on the potential energy surface.

Determination of acid association constants: Ground-state acid association constants (K) of the ADCA derivatives were determined via absorption spectroscopy by monitoring the change in

absorption (corrected for dilution) as a function of added acid concentration. Samples of the three acids were prepared in solutions of water with 0, 10 and 30 mol% DMF and were titrated using NaOH and HCl. The absorption value near the isosbestic point at each addition of acid was plotted as a function of acid concentration and the data was fit to Eq. (1),

$$A_i = \frac{A_{max}[H^+]^n + A_{min}K}{K + [H^+]^n} \quad (1)$$

where A_i is the absorbance at a given concentration of acetic acid, A_{max} and A_{min} are the absorbance values for the fully protonated and deprotonated species, respectively, and n is the number of protons associated with a given acid association constant, K. A_i values were fit to Eq. (1) with K as a variable parameter. Fixing n to 2 yielded the most reasonable fit of the data. The p K values were plotted versus mol% DMF, and the p K value of each compound in pure DMF was determined by extrapolating to 100 mol% DMF (Figs. S10–S12). Excited-state acid association constants (p K^*) were predicted using the Förster cycle, (Eq. (2)),

$$pK^* - pK = 2.1 \times 10^{-3}(\bar{\nu}_{A^-} - \bar{\nu}_{AH}) \quad (2)$$

$$\bar{\nu}_{0-0} = \frac{\bar{\nu}^{abs}_{max} - \bar{\nu}^{em}_{max}}{2} \quad (3)$$

where $\bar{\nu}_{A^-}$ and $\bar{\nu}_{AH}$ correspond to the wavenumber of the 0–0 transitions of A^- and AH, respectively. The wavenumber corresponding to the 0–0 transition was estimated by averaging the wavenumbers at the absorption and emission maxima (Eq. (3))[4].

3. Results

The steady-state absorption and emission spectra of 2,6-ADCA (a,b), 1,4-ADCA (c,d) and 9,10-ADCA (e,f) measured in THF are shown in Fig. 2. 2,6-ADCA displays vibronically structured absorption and emission bands. Although the structure of the

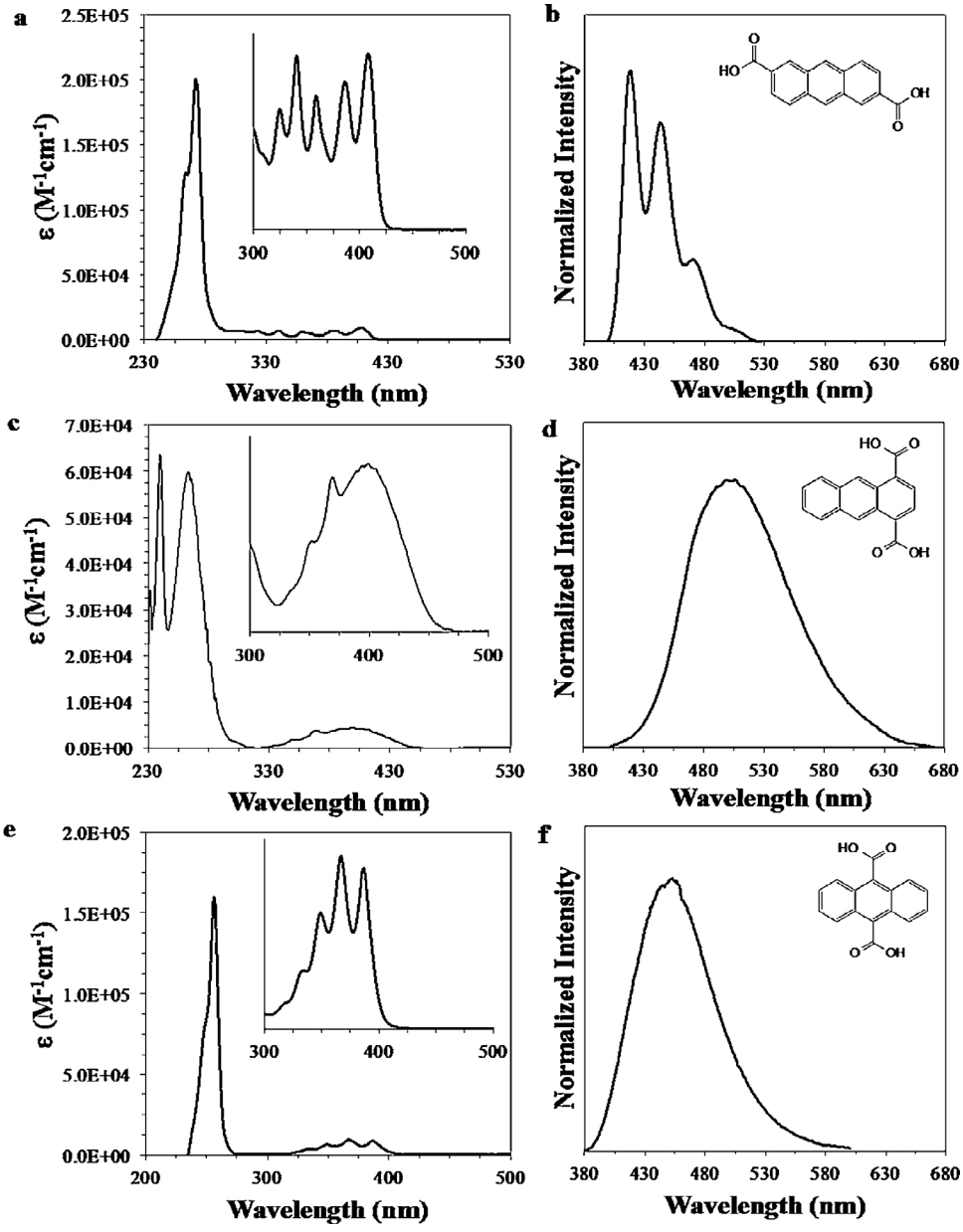

Fig. 2. Absorption (left) and emission spectra (right) of 2,6-ADCA (a,b) 1,4-ADCA (c,d) and 9,10-ADCA (e,f) in THF.

emission spectrum closely resembles that of anthracene, the absorption spectrum differs from anthracene in both the number of lower-energy (~320 nm – 420 nm for 2,6-ADCA and 285 nm–385 nm for anthracene) absorption bands and their intensities. The absorption spectrum of 1,4-ADCA appears broad with subtle structural features at 360 nm and 370 nm, and the emission spectrum is broad and structureless. 9,10-ADCA exhibits a vibronically structured absorption band, similar in shape to that of anthracene, while the emission spectrum is broad and diffuse. Both the absorption and emission spectra of each derivative are bathochromically shifted relative to anthracene (Table 1). Additionally, the $^1A \rightarrow {}^1B_b$ absorption peak of 1,4-ADCA at 240 nm is significantly broadened relative to anthracene and is split into two peaks. 2,6-ADCA exhibits a Stokes shift (584 cm^{-1} in THF) that is slightly larger than that of anthracene (208 cm^{-1} in THF). 1,4-ADCA and 9,10-ADCA display large Stokes shifts (4803 cm^{-1} and 3667 cm^{-1} in THF) compared to anthracene. The observed lifetimes of each isomer in THF are considerably longer than the 4.9 ± 0.1 ns fluorescence lifetime of anthracene in the same solvent (Table 2).

In order to probe the effects of solvent polarity on the photophysical properties of the anthracene derivatives, the absorption and emission spectra as well as the lifetimes and quantum yields were measured in a series of polar aprotic solvents. Table 1 and Table S1 summarize the spectral data and Stokes shifts of the three isomers in various solvents. The Stokes shift was calculated from the 0–0 transition band in the vibronically structured spectra and from the maximum of the diffuse spectra. Neither the absorption nor emission spectra of 9,10-ADCA are affected by solvent polarity. The absorption spectrum of 9,10-ADCA displays anthracene-like vibrational structure in all neat solvents tested. The emission spectrum is broad and diffuse with a λ^{em}_{max} around 455 nm in neat solvents, in which λ^{em}_{max} is bathochromically shifted by 14 nm (Fig. S3, Table S1). The average observed Stokes shift is 3796 cm^{-1} ± 114 in THF, ethyl acetate, butanone, acetone and DMA (Table S1). Similarly, solvent polarity has no significant effect on the absorption or emission spectra of 2,6-ADCA, as the maxima do not shift significantly between THF (ε = 7, λ^{abs}_{max} = 409 nm, λ^{em}_{max} = 419 nm), and DMA (ε = 38, λ^{abs}_{max} = 408 nm, λ^{em}_{max} = 421 nm, Fig. S1, Table S1). In contrast to the other two isomers, the absorption band of 1,4-ADCA is hypsochromically shifted by 10 nm, from 396 nm in THF (ε = 7) to 386 nm for DMA (ε = 38, Fig. S2, Table S1), and the emission maximum is bathochromically shifted by 8 nm from 498 nm in THF to 497 nm in DMA. The absorption and emission spectra of 1,4-ADCA remain broad and diffuse in all of the neat solvents explored.

Table 1
Summary of absorption and emission data for the ADCAs.

	Solvent	λ^{abs}_{max} (nm)	λ^{em}_{max} (nm)	Stokes (cm^{-1})
2,6-ADCA	THF	409	419	584
	Acidic DMF	409	423	809
	Basic DMF	392	400	510
1,4-ADCA	THF	396	498	4803
	Acidic DMF	390	522	6484
	Basic DMF	396	430	1997
9,10-ADCA	THF	387	451	3667
	Acidic DMF	389	451	3534
	Basic DMF	400	410	610
Anthracene	THF	358	397	274

λ^{abs}_{max} is the lowest energy maximum in the absorbance spectrum, and λ^{em}_{max} is the highest energy maximum in the fluorescence spectrum. The Stokes shift was calculated from the 0–0 transition band in the vibronically structured spectra and from the maximum of the diffuse spectra.

The fluorescence quantum yields (Φ_{fl}) and fluorescence lifetimes (τ_f), along with the radiative (k_r) and non-radiative (k_{nr}) rate constants for the three ADCA derivatives in the various solvents, are listed in Table 2 and Table S2. No trends are observed between solvent polarity and fluorescence quantum yields over the solvent series (Table S2). In general, the fluorescence lifetimes are largely independent of solvent polarity but are considerably shorter in basic conditions [17–20].

To further explore how the protonation state of the carboxylic acid substituents affects the excited-state properties of the anthracene derivatives, photophysical measurements were carried out in acidic DMF and basic DMF (Fig. 3, Table 2). All three isomers exhibit anthracene-like vibronic structure in the absorption spectra recorded in basic DMF. The emission spectrum of 2,6-ADCA displays more defined vibronic structure in basic solution compared to acidic. The emission spectrum of 1,4-ADCA remains broad and structureless in both basic and acidic environments. On the other hand, 9,10-ADCA exhibits a broad, diffuse emission spectrum in acidic DMF, but in basic DMF, anthracenic vibronic structure is observed. The absorption spectra of 1,4-ADCA and 9,10-ADCA are hypsochromically shifted in basic DMF relative to acidic, while that of 2,6-ADCA is bathochromically shifted in basic solution. Additionally, the emission spectrum of each of the derivatives is hypsochromically shifted under basic conditions compared to acidic. The Stokes shifts decrease considerably with solvent pH, going from 809 cm^{-1} to 510 cm^{-1} for 2,6-ADCA, 6484 cm^{-1} to 1997 cm^{-1} for 1,4-ADCA, and from 3534 cm^{-1} to 610 cm^{-1} for 9,10-ADCA (Table 1). The quantum yields of 2,6-ADCA and 1,4-ADCA decrease considerably under basic conditions compared to acidic solution, while that of 9,10-ADCA decreases only by about half (Table 2).

To quantify the degree of protonation in both the ground and excited states as a function of pH, the ground-state acid association constants (K) of the ADCAs were determined by absorption spectroscopy (Figs. S10–S12, equation 2), and pK values of 17.6, 17.9 and 19.4, for 2,6-ADCA, 1,4-ADCA and 9,10-ADCA, respectively, were obtained in the ground state. The excited-state acid association constants (pK^*) were then calculated in DMF from the Förster cycle (*vide supra*) and found to be 23.0, 23.2 and 23.8, accordingly. Thus, in neutral solutions, the ADCA derivatives are predominantly protonated in both the ground state and the excited state.

In addition to solvent polarity and protonation state, geometry can have a significant effect on photophysical properties. DFT and TDDFT calculations were performed to obtain the energies and geometries of the three compounds as a function of the dihedral angles (see Fig. S8 for a definition of the dihedral angles) between the carboxylic acid groups and the anthracene ring system (Fig. 4) both in the ground state and in the excited state. The potential energy contours for the 2,6-ADCA isomer in the ground state (Fig. 4a) show that the lowest-energy conformation occurs when the carboxylic acids and the anthracene moiety are coplanar. In the excited state, the lowest-energy geometry does not change with respect to the ground state, and the molecule remains planar (Fig. 4b). Similar results are obtained for the 1,4-ADCA isomer, where coplanarity of the carboxylic acids and anthracene moieties is observed in both the ground (Fig. 4c) and the first excited state (Fig. 4d). On the other hand, the results for the 9,10-ADCA isomer are strikingly different (Fig. 4e, and f). For this isomer, the lowest-energy conformation does not exhibit the carboxylic acids in the same plane as the aromatic rings in either the ground or the first excited state. Full geometry optimizations reveal that the lowest-energy structure for the ground state 9,10-isomer has dihedral angles of 56.6°, and these dihedrals decrease to 27.7° in the first excited state (Fig. 5). Furthermore, the anthracene moiety in the

Table 2
Summary of the lifetime and quantum yield data for ADCAs.

	Solvent	τ_f (ns)	τ_0 (ns)	Φ_f	k_r ($10^{-7}s^{-1}$)	k_{nr} ($10^{-7}s^{-1}$)
2,6-ADCA	THF	12.3 ± 0.7	15.8 ± 0.08	0.78 ± 0.074	0.063	0.018
	Acidic DMF	12.5 ± 0.4	14.6 ± 0.1	0.82 ± 0.080	0.068	0.015
	Basic DMF	2.9 ± 0.02	26.4 ± 0.03	0.11 ± 0.018	0.038	0.307
1,4-ADCA	THF	19.2 ± 1.0	31.5 ±0.1	0.61 ± 0.068	0.032	0.020
	Acidic DMF	12.5 ± 0.1	32.1 ± 0.2	0.19 ± 0.042	0.031	0.049
	Basic DMF	1.0 ± 0.1	15.2 ± 0.6	0.066 ± 0.015	0.066	0.930
9,10-ADCA	THF	8.8 ± 0.1	13.3 ± 0.2	0.66 ± 0.085	0.075	0.039
	Acidc DMF	5.7 ±0.3	14.3 ± 0.1	0.40 ± 0.05	0.070	0.110
	Basic DMF	2.2 ± 0.04	11.6 ± 0.4	0.19 ± 0.015	0.086	0.370
Anthracene	THF	4.9 ± 0.1	12.3 ± 0.05	0.40 ± 0.01	0.082	0.120

τ_f is the fluorescence lifetime, τ_0 is the singlet-excited state lifetime, Φ_f is the fluorescence quantum yield, and k_r and k_{nr} are the rates of radiative and non-radiative decay, respectively.

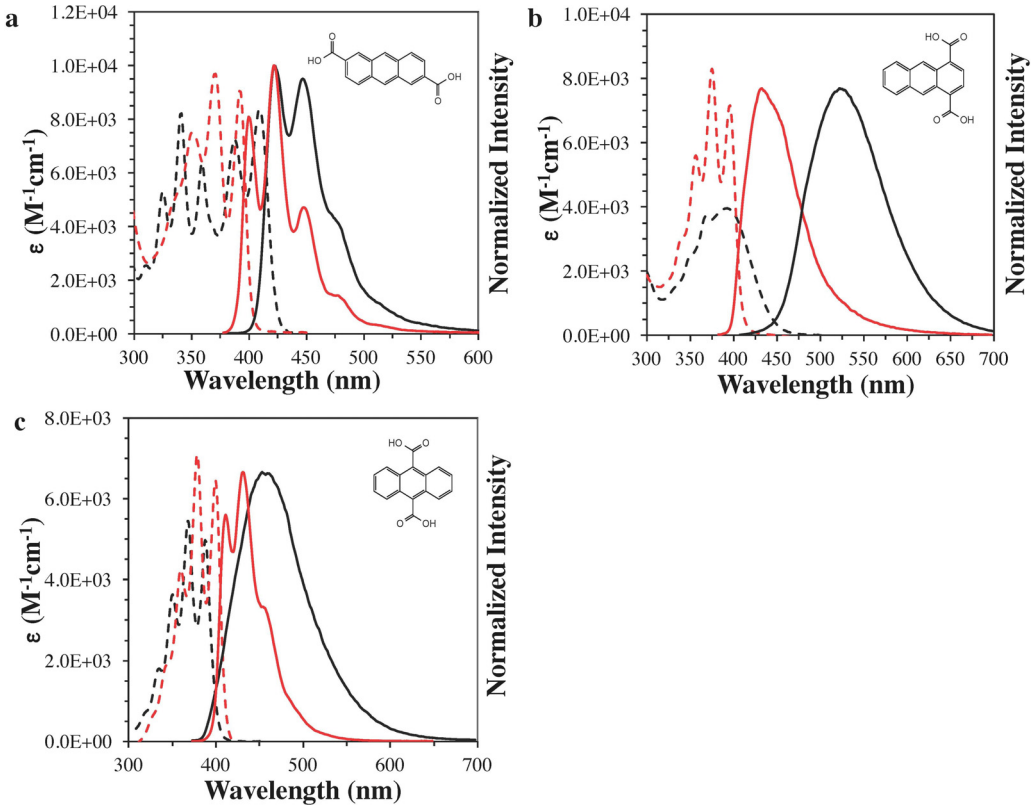

Fig. 3. Absorption and emission spectra of 2,6-ADCA (a), 1,4-ADCA (b) and 9,10-ADCA (c) acidic DMF (black) and basic DMF (red). (For interpretation of the references to colour in this figure legend, the reader is referred to the web version of this article.)

9,10-isomers seems to undergo a noticeable puckering upon excitation that is completely absent in the other two isomers.

Close examination of the energy contours in Fig. 4 reveals that, interestingly, there seems to be a lower barrier for carboxyl rotation for 1,4-ADCA than for 2,6-ADCA in the ground state. Indeed, when one of the carboxylic acid groups is coplanar to the anthracene moiety, the barrier for full rotation of the other carboxylic acid group is about 5.5 kcal/mol in 1,4-ADCA, but around 8 kcal/mol in 2,6-ADCA. The most energetically favorable conformations of both 2,6-ADCA and 1,4-ADCA have dihedral angles of θ = 0°, and both have a maximum energy when θ = 90°.

Finally, molecular orbital calculations from DFT as well as excitation data from TDDFT reveal that, for each isomer in both the protonated and deprotonated state, the lowest-energy singlet transition has mainly a HOMO-LUMO contribution. Fig. S19 shows frontier orbital density plots for each molecule, calculated using the minimum-energy geometry at the ground state. For the protonated anthracene carboxylic acid derivatives, calculated oscillator strengths remain on the same order of magnitude for this transition regardless of carboxylic acid dihedral angle (2,6-ADCA: 0.05-0.07; 1,4-ADCA: 0.05-0.08; 9,10-ADCA: 0.09-0.11). For the deprotonated isomers, oscillator strengths for the ground- to first-excited state transition peak at values of 0.09 for 2,6-ADCA^{2-}, 0.03 for 1,4-ADCA^{2-}, and 0.07 for 9,10-ADCA^{2-}, and become increasingly small as the dihedral angles approach 0°.

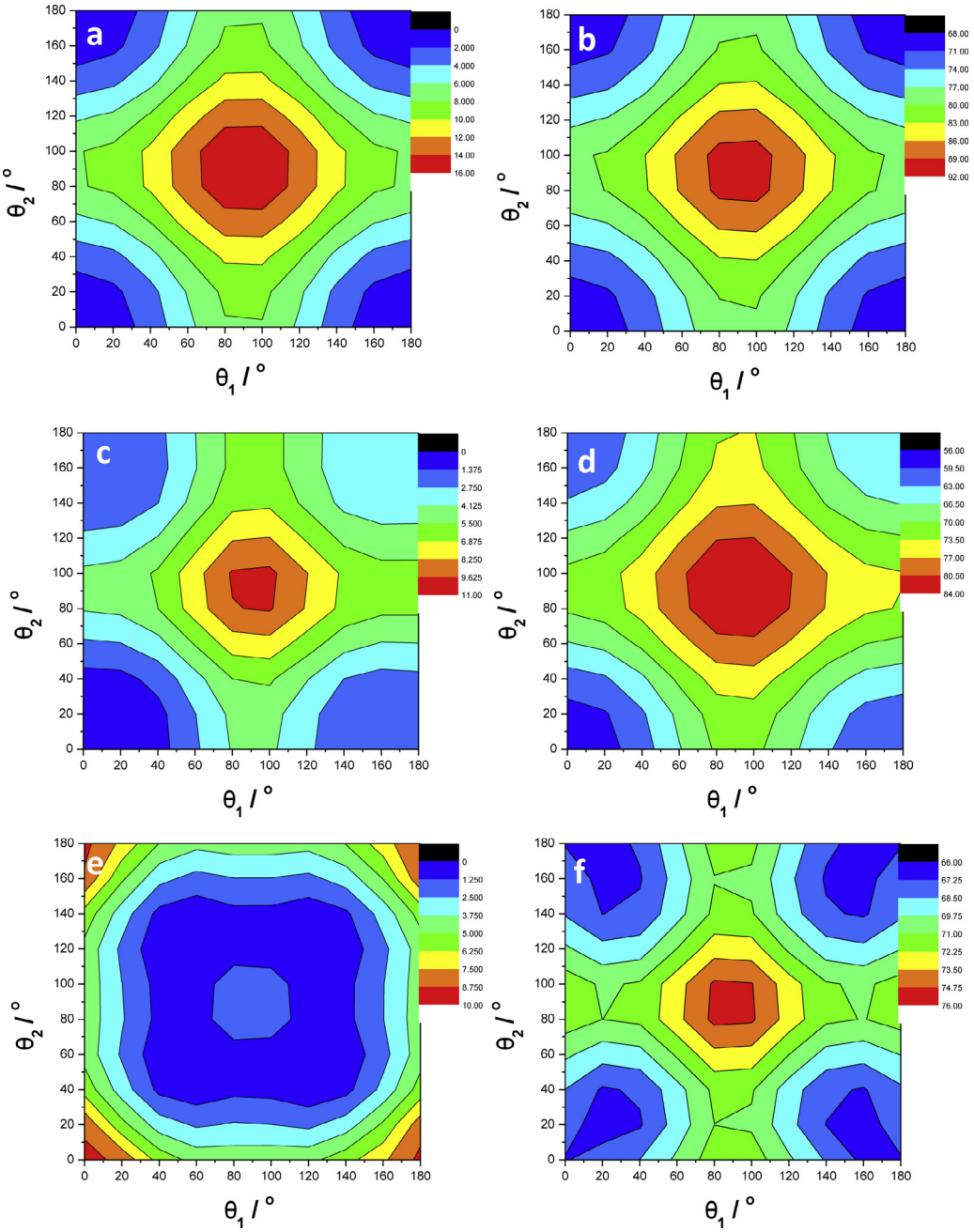

Fig. 4. DFT-calculated energies as a function of dihedral angles between —COOH groups and anthracene. Ground state of 2,6-ADCA (a), 1,4-ADCA (c), and 9,10-ADCA (e), and first excited state of 2,6-ADCA (b), 1,4-ADCA (d), and 9,10-ADCA (f). Energy scales for each plot are shown in kcal/mol relative to the minimum energy of the ground state. (See Fig. S8 for a definition of the dihedral angles.).

4. Discussion

As expected, the photophysical characteristics of anthracene are sensitive to the position of the carboxylic acid functionalities on the ring system. Additionally, the protonation state of the acid groups further alters the excited-state properties of each anthracene derivative. The question then becomes, what is the main process that governs the photophysics of each isomer: acid-base equilibrium, solvent, formation of higher order aggregates, or excited-state structural reorganization?

Neither solvent polarity nor hydrogen bonding character alters the photophysics of 2,6-ADCA. Thus, it is unlikely that intermolecular interactions play a significant role in altering the excited-state properties of the anthracene moiety of this isomer. In basic solution, the vibrational structure of the absorption spectrum closely resembles that of the unsubstituted anthracene molecule. On the other hand, the absorption spectra recorded in acidic and neat solvents display a distinct vibronic structure, different from that of observed for anthracene. In previous literature reports of the mono-substituted, 2-napthalene carboxylic acid (2-NCA) and 2-anthracenecarboxylic acid (2-ACA), a similar distinct vibronic structure in the absorption spectrum to that measured for the di-substituted 2,6-ADCA in neat and acidic solution was observed [35]. The phenomenon was attributed to stabilization of the $^1A \rightarrow {}^1L_b$ longitudinally polarized low-energy transition. The $^1A \rightarrow {}^1L_b$ transition is weak in unsubstituted anthracene, and the corresponding absorption bands are obscured by the more intense transversely polarized $^1A \rightarrow {}^1L_a$ absorption bands. The di-

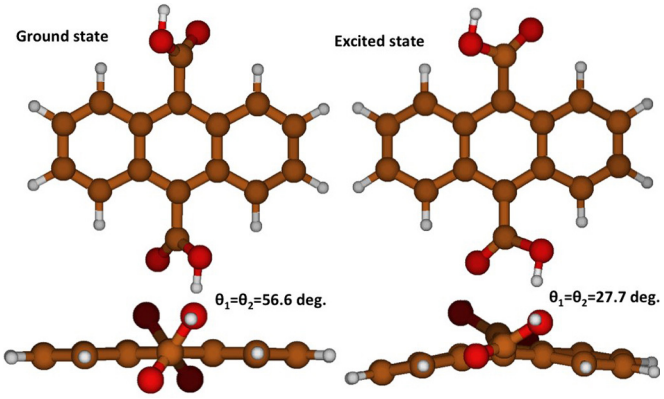

Fig. 5. DFT calculated lowest-energy structures of the 9,10-ADCA molecule in the ground state (left) and the first excited state (right).

substituted, 2,6-ADCA, studied herein, further extends the length of the molecule, resulting in greater stabilization of the $^1A \rightarrow {}^1L_b$ transition. Accordingly, the bands assigned to $^1A \rightarrow {}^1L_b$ appear with greater intensity in the absorbance spectrum of 2,6-ADCA, as compared to both unsubstituted anthracene and 2-ACA. DFT calculations of the lowest energy ground-state configuration of 2,6-ADCA suggest a coplanar arrangement between the carboxylic acids and the anthracene macrocycle (Fig. 4a). This is in agreement with that observed in crystal structures of 2-ACA [44]. The coplanar arrangement allows for resonance interactions between the acid groups and the aromatic ring system to occur. These resonance interactions increase the dipole moment, and thus, the oscillator strength of the $^1A \rightarrow {}^1L_b$ transition, resulting in the appearance of the $^1A \rightarrow {}^1L_b$ bands [35]. Further, TDDFT calculations of 2,6-ADCA show that vertical excitation from the ground to first excited state is almost entirely contributed by a HOMO-LUMO transition; the molecular orbitals for both states are shown in Fig. S19a. These orbitals show polarization along the long axis of the molecule upon excitation, as electron density shifts into the carboxylic acid moieties upon excitation.

The emission spectrum of 2,6-ADCA in neutral and acidic solutions is not a mirror image of the absorbance spectrum. Although it displays anthracenic vibronic structure in all solvent conditions, the number of vibronic transitions in the emission spectrum is reduced compared to the absorption spectrum. This is not entirely unexpected, as ^1L_a is the only emissive state, and the additional vibronic structure is assumed to be due to absorption into the ^1L_b state [45]. The vibronic structure is indicative of little intermolecular reorganization in the excited state. Accordingly, the fluorescence spectrum measured at 77 K also displays vibronic structure, and the emission bands are not shifted from the spectrum recorded at room temperature (Fig. S7a, Table S3). The slight bathochromic shift in the absorption spectrum relative to anthracene is attributed to inductive effects imposed by the presence of the electron withdrawing functional groups on the polyaromatic ring.

At higher pH values, the carboxylate groups of 2,6-ADCA are less likely to participate in resonance interactions, leading to further decoupling from the aromatic ring system and giving rise to anthracenic vibronic structure in the absorption spectrum [46]. Indeed, the vibronic structure in the absorbance spectrum of deprotonated 2,6-ADCA^{2-} more closely resembles that of anthracene, but is bathochromically shifted ~19 nm relative to anthracene. Thus, the carboxylic acid groups affect the aromatic system through inductive effects but do not participate in resonance interactions when deprotonated.

Contrary to 2,6-ADCA, both the absorption and emission spectra of 1,4-ADCA in neutral solvents lack vibronic structure and are diffuse [45]. Similar observations have been reported for 1-anthracenecarboxylic acid (1-ACA) [45]. DFT calculations conducted in this study for the disubstituted, 1,4-ADCA predict a lowest energy ground state geometry in which the carboxylic acid groups are coplanar with anthracene (Fig. 4c). This conformation increases resonance interactions between the overlapping orbitals of the π-system and carboxyl groups, introducing charge-transfer (CT) character into the $^1A \rightarrow {}^1L_a$ transition (polarized along the short axis), and electron density shifts toward the functionalized ring. Orbital density plots of the HOMO and LUMO of 1,4-ADCA, shown in Fig. S19b, confirm this shift during electronic excitation. The resulting shift of electron density results in loss of vibronic structure in both the absorption and emission spectra. The magnitude of the Stokes shift of 1,4-ADCA increases with the polarity of the solvent, i.e. THF < DMF ≈ DMA. Closer inspection of the spectroscopic data reveals that, as solvent polarity increases, an overall bathochromic shift of ~19 nm is observed in the emission spectrum. Because the carboxyl groups of 1,4-ADCA introduce CT character into the $^1A \rightarrow {}^1L_a$ transition, the absorption spectrum is sensitive to solvent interactions with the functional groups. As solvent polarity increases, the excited state is stabilized due to solvent-solute induced dipolar interactions, giving rise to the bathochromic shift observed in the emission spectrum [45,47]. Therefore, solvent relaxation about the weaker excited-state dipole likely contributes to the large Stokes shifts. The emission spectrum recorded at 77 K remains unstructured, but is bathochromically shifted from 498 nm to 465 nm, due to hindered vibronic relaxation (solvent and/or substituent) in the glass matrix (Fig. S7b, Table S3). The coplanar arrangement of the carboxylic acids in the ground state, along with the lack of vibronic structure in the emission spectrum, suggests that the resonance interactions between the carboxylic acids and aromatic ring system in the ground state are conserved in the excited state. This is corroborated by the coplanar lowest-energy structure found in the first excited state (Fig. 4d).

In basic solution, the absorbance spectrum of 1,4-ADCA^{2-} is vibronically structured, while the emission spectrum is still broad and diffuse. The deprotonated carboxyl groups do not contribute to resonance forms of the anion in the ground state and, consequently, the absorbance spectra are vibronically structured. The predominance of electron density in the carboxylate groups and sparseness of density in the anthracene moiety in the DFT-calculated HOMO, shown in Fig. S19e, confirm this lack of resonance contribution. There are several factors that may contribute to the loss of structure in the emission spectrum. As previously proposed for 1-ACA$^-$, the authors attribute the broadening of the emission spectrum to a shift in electron density upon promotion to the ^1L_a excited state. The orbital density plot of the LUMO shows agreement with this proposition for 1,4-ADCA^{2-}, as this excited state shows strong population in the anthracene moiety. Such a shift in electron density in the direction of the carboxylate group introduces some CT character between the functional group and anthracene moiety [45]. It is plausible that such phenomena also contribute to the loss of structure observed in the emission spectrum of 1,4-ADCA^{2-}. The Stokes shift of 1,4-ADCA^{2-} (1997 cm^{-1}) is large in comparison with the deprotonated 2,6-ADCA^{2-} (510 cm^{-1}) and 9,10-ADCA^{2-} (610 cm^{-1}). A relatively large change in molecular dipole moment upon excitation would result in such a substantial Stokes shift. Solvent relaxation may also have a significant effect on the fluorescence spectrum. Because the energy of the relaxed excited state is lower than that of the initial Frank-Condon excited state, thermodynamic equilibration with the surrounding solvent would contribute to the loss of structure and bathochromic shift in the emission spectrum of 1,4-ADCA^{2-}. Lastly, it is likely that the carboxylate groups can easily rotate, which would also give rise to a large Stokes shift (relative to both 2,6-

ADCA^{2-} and 9,10-ADCA^{2-}) and broad emission spectrum due to nuclear reorganization. The energy contour plot for the first excited state of 1,4-ADCA^{2-}, shown in Fig. S9f, confirms this. In this state, the potential surface is rather isotropic and large (essentially free) dihedral rotation can occur. Analogous free-rotation regions for 2,6-ADCA^{2-} and 9,10-ADCA^{2-}, shown in Figs. S9b and d, respectively are much smaller, suggesting that these excited states have more confined geometries than 1,4-ADCA^{2-}.

In neat solvents, the absorption spectrum of 9,10-ADCA displays anthracenic vibronic structure, while the emission spectrum is characterized by a broad, structureless band. Similar observations have been reported for 9-anthracenecarboxylic acid (9-ACA) [26,27,48]. The structureless emission of 9-ACA was ascribed to enhanced resonance interactions between the carboxylic acid group and the aromatic moiety, due to rotation of the functional group into the plane of the ring system following excitation [23].

DFT calculations of the lowest energy configuration ground-state geometry of 9,10-ADCA reveal a dihedral angle of 57° between the carboxylic acid groups and anthracene plane. Comparably, 9-ACA was found to have a dihedral angle of 57°, and 88° for the conjugate base, 9-ACA^{-} [27]. This ground-state configuration of 9-ACA is supported by crystallographic data [42]. The non-planar geometry has been attributed to steric interactions between the acid group and the peri-hydrogens on the carbons in the 1 and 8 positions of the anthracene ring [23]. The non-planar orientation prevents resonance interactions between the carboxylate groups and aromatic ring system, and gives rise to anthracene-like vibronic structure in the absorption spectrum. The orbital density plot of the 9,10-ADCA HOMO (Fig. S19c) confirms this rationale, as there appears to be very little electron density on the carboxylic acid moiety in this state. The inductive effects of the electron withdrawing carboxylic acid groups result in the slight bathochromic shift observed in the absorption spectrum of 9,10-ADCA relative to anthracene. Deprotonation of the carboxylic acids reduces the strength of the inductive effects and, consequently, the bathochromic shift in the absorption spectrum of 9,10-ADCA^{2-} is smaller.

TDDFT calculations show that the dihedral angle, θ, decreases to ~28° in the excited state of 9,10-ADCA (Fig. 4f). Interestingly, as the carboxyl groups twist toward a more coplanar orientation, the anthracene ring also puckers. Previously, a θ of ~33° was calculated by TDDFT for 9-ACA in the excited state, but no ring distortion was reported [27]. The distortion of the anthracene plane, observed in 9,10-ADCA but not 9-ACA, may be due to greater steric strain on the molecule imposed by the additional carboxylic acid. Puckering of the anthracene ring system upon rotation of the carboxyl groups disrupts the transition dipole moment across the short-axis. The large reconfiguration energies associated with this rotation and nuclear reorganization lower the energy of the excited state, as evidenced by the large Stokes shift observed in the spectra of 9,10-ADCA. The more coplanar orientation allows for overlapping of the p-orbital of the acid group with the π-aromatic system of anthracene, introducing resonance interactions through delocalization of electron density from anthracene into the carboxyl substituents. This significantly perturbs the $^1A \rightarrow {}^1L_a$ transition dipole moment oriented along the short axis of anthracene, giving rise to a broad, structureless emission band. At 77 K, when rotation of the carboxylic acid groups is hindered, the emission spectrum of 9,10-ADCA is bathochromically shifted ~25 nm and displays some vibronic structure (Fig. S7c, Table S3). With increased resonance interactions, solvent-solute interactions have a greater contribution to the Stokes shift depending on the rate of rotation of the carboxyl groups relative to the rate of solvent reorganization as intramolecular nuclear reorganization occurs in the excited state. The mirror-image relationship between the absorption and emission spectra of the fully deprotonated 9,10-ACA^{2-} measured in basic solution indicates that the geometries of the ground and excited states of 9,10-ACA^{2-} are almost identical. Thus, the carboxylate groups remain decoupled from the aromatic system, resulting in vibronically structured emission. This is also supported by DFT/TDDFT calculations, which show little changes between the dihedral angles of 9,10-ADCA^{2-} in the ground (Fig. S9c) and excited (Fig. S9d) states.

5. Conclusions

Functionalization of anthracene with carboxylic acid groups results in perturbation of the photophysical properties depending on both the location of the groups and extent of their interaction with the aromatic ring system. In general, functionalization that extends the molecule along the molecular axes containing optical transitions of the same polarization affect the properties of that transition more significantly. For example, derivatization at the 2 and 6 positions extends the molecule along the longitudinal axis and enhances the longitudinally polarized $^1A \rightarrow {}^1L_b$ transition, giving rise to intense $^1A \rightarrow {}^1L_b$ absorption bands. In the 2,6-isomer, electron density remains evenly distributed in the molecule and vibronically structured absorption bands are observed. On the other hand, functionalization at the 1 and 4 positions, which lengthens the molecule along the short axis, gives rise to an uneven distribution of electron density along the polyaromatic ring system and results in broad, diffuse bands in both the absorption and emission spectra. The extent of interaction between the carboxylic acids and the anthracene ring is dictated by how the functional groups are oriented with respect to the anthracene plane. In 1,4-ADCA, the carboxyl groups lie coplanar with the parent anthracene, but in 9,10-ADCA, steric hindrances prevent coplanarity. As a result, there is greater overlap between the p orbitals of the acid groups in the 1 and 4 positions with the π orbitals of anthracene, introducing a greater amount of charge transfer character in 1,4-ADCA compared to 9,10-ADCA. Accordingly, the photophysical properties of 1,4-ADCA are also sensitive to solvent-solute interactions and exhibit a dependence upon solvent polarity. The solvent pH also has a significant influence on the extent to which the functional groups interact with the ring system. In very basic solutions, where the carboxyl groups are completely deprotonated and cannot participate in resonance interactions, vibronically structured bands are observed in the absorbance spectra of all of the ADCA derivatives.

This work provides insight into the structure-property relationship of dicarboxylic anthracene derivatives and their fluorescent properties. An understanding of the effects of substitutions and local environment on the excited-state properties of anthracene can be used to further tune derivatives to obtain desired functionality. Such knowledge will aid in the design of next-generation optoelectronic materials.

Acknowledgements

This material is based upon work supported by the U.S. department of Energy, Office of Basic Energy Sciences under Award Number DE-SC0012446. The authors acknowledge Advanced Research Computing at Virginia Tech for providing computational resources and technical support that have contributed to the results reported within this paper.

Appendix A. Supplementary data

Supplementary data associated with this article can be found, in the online version, at http://dx.doi.org/10.1016/j.jphotochem.2016.12.021.

References

[1] M.Y. Zhu, C. Yang, Blue fluorescent emitters: design tactics and applications in organic light-emitting diodes, Chem. Soc. Rev. 42 (2013) 4963–4976.
[2] N.S. Kaur, M. Singh, D. Pathakc, T. Wagner, J.M. Nunzi, Organic materials for photovoltaic applications: review and mechanism, Synth. Met. 190 (2014) 20–26.
[3] Y. Wakayama, R. Hayakawa, H.S. Seo, Recent progress in photoactive field-effect transistors, Sci. Technol. Adv. Mater. 15 (2014) 1019.
[4] S.A. van de Linde, C. Franke, T. Holm, T. Klein, A. Löschberger, S. Proppert, S. Wolter, M. Sauer, Investigating cellular structures at the nanoscale with organic fluorophores, Chem. Biol. 20 (2013) 8–18.
[5] J.W. Sidman, Electronic and vibrational states of anthracene, J. Chem. Phys. 25 (1956) 115–121.
[6] B.K.N. Shah, D.C. Neckers, J. Shi, E.W. Forsythe, D. Morton, Photophysical properties of anthanthrene-based tunable blue emitters, J. Phys. Chem. A 109 (2005) 7677–7681.
[7] J.N. Moorthy, P. Venkatakrishnan, P. Natarajan, D.F. Huang, T.J. Chow, De novo design for functional amorphous materials: synthesis and thermal and light-emitting properties of twisted anthracene-functionalized bimesitylenes, J. Am. Chem. Soc. 130 (2008) 17320.
[8] S.X. Tao, X. Zhang, Efficient blue organic light-emitting devices based on novel anthracene derivatives with pronounced thermal stability and excellent film-forming property, Chem. Phys. Lett. 429 (2006) 622–627.
[9] T.M. Swager, C.J. Gil, M.S. Wrighton, Fluorescence studies of poly(p-phenyleneethynylene)s: the effect of anthracene substitution, J. Phys. Chem. 99 (1995) 4886–4893.
[10] J.R. Platt, The box model and electron densities in conjugated systems, J. Chem. Phys. 22 (1954) 1448–1455.
[11] H.B. Klevens, J.R. Platt, Spectral resemblances of cata-condensed hydrocarbons, J. Chem. Phys 17 (1949) 470–483.
[12] J.R. Platt, Classification of spectra of cata-condensed hydrocarbons, J. Chem. Phys. 17 (1949) 484–495.
[13] J.R. Lackowicz, Principles of Fluorescence Spectroscopy, 3rd ed., Springer Science + Business Media, LLC, 2010, pp. 32.
[14] I.R. Tigoianu, A. Airinei, D.O. Dorohoi, Solvent influence on the electronic fluorescence spectra of anthracene, Rev. Chim. (Bucharest, Rom.) 61 (2010) 491–494.
[15] B. Valeur, M.N. Berberan-Santos, Molecular Fluorescence: Principles and Applications, Wiley-VCH, 2012, pp. 77.
[16] I.B. Berlman, Handbook of Fluorescence Spectra of Aromatic Molecules, 2d ed., Academic Press, New York, 1971, pp. 57–59.
[17] W.H. Melhuish, Quantum efficiencies of fluorescence of organic substances: effect of solvent and concentration of the fluorescent solute, J. Phys. Chem. 65 (1961) 229–235.
[18] W.R. Ware, B.A. Baldwin, Absorption intensity and fluorescence lifetimes of molecules, J. Chem. Phys. 40 (1964) 1703.
[19] W.R. Dawson, M.W. Windsor, Fluorescence yields of aromatic compounds, J. Phys. Chem. 72 (1968) 3251.
[20] R.A. Lampert, L.A. Chewter, D. Phillips, D.V. O'Connor, A.J. Roberts, S.R. Meech, Standards for nanosecond fluorescence decay time measurements, Anal. Chem. 55 (1983) 68–73.
[21] I. Momiji, C. Yoza, K. Matsui, Fluorescence spectra of 9-anthracenecarboxylic acid in heterogeneous environments, J. Phys. Chem. B 104 (2000) 1552–1555.
[22] M.S.A. Abdel-Mottaleb, H.R. Galal, A.F.M. Dessouky, M. El-Naggar, D. Mekkawi, S.S. Ali, G.M. Attya, Fluorescence and photostability studies of anthracene-9-carboxylic acid in different media, Int. J. Photoenergy 2 (2000) 48–53.
[23] T.C. Werner, D.M. Hercules, Fluorescence of 9-anthroic acid and its esters Environmental effects on excited-state behavior, J. Phys. Chem. 73 (1969) 2005–2011.
[24] S. Suzuki, T. Fujii, N. Yoshiike, S. Komatsu, T. Iida, Absorption and fluorescence spectra of anthracenecarboxylic acids I. 9-Anthroic acid and formation of excimer, Bull. Chem. Soc. Jpn. 51 (1978) 2460–2466.
[25] N. Bazilevskaya, A. Cherkasov, Two fluorescence bands of mesoanthracenecarboxylic acids and excimers, Appl. Spectrosc. 3 (1965) 412–416.
[26] N. Ghoneim, D. Scherrer, P. Suppan, Dual luminescence, structure and eximers of 9-anthracene carboxylic acid, J. Lumin. 55 (1993) 271–275.
[27] W. Rodriguez-Cordoba, R. Noria-Moreno, P. Navarro, J. Peon, Ultrafast fluorescence study of the effect of carboxylic and carboxylate substituents on the excited state properties of anthracene, J. Lumin. 145 (2014) 697–707.
[28] A.G. Cabellero, A.K. Croft, S.M. Nalli, Remote aromatic stabilization in radical reactions, Tetrahedron Lett. 49 (2008) 3613–3615.
[29] S.A. Fontenot, M.A.W. Cangelosi, A.C. Pitt, L.N. Sather, O.B. Berryman, D.W. Johnson, Design, synthesis and characterization of self-assembled As_2L_3 and Sb_2L_3 cryptands, Dalton Trans. 40 (2011) 12125–12131.
[30] R.O. Garay, H. Naarmann, K. Mullen, Synthesis and characterization of poly (1,4-anthrylenevinylene), Macromolecules 27 (1994) 1922–1927.
[31] J.P. Arient, Nitration and oxidation of anthraquinone dimethyl derivatives, Collect, Czech. Chem. Commun. 39 (1973) 3117.
[32] S. Jones, J.C. Atherton, M.R.J. Elsegooda, W. Clegga, Dimethyl 9,10-anthracenedicarboxylate: a centrosymmetric transoid molecule, Acta. Cyst. C 56 (2000) 881–883.
[33] D.V. O'Connor, D. Phillips (1984), Time–correlated Single Photon Counting, Academic Press, London, 2016, pp. 36–54.
[34] M.J. Frisch, G.W. Trucks, H.B. Schlegel, G.E. Scuseria, M.A. Robb, J.R. Cheeseman, G. Scalmani, V. Barone, B. Mennucci, G.A. Petersson, H. Nakatsuji, M. Caricato, X. Li, H.P. Hratchian, A.F. Izmaylov, J. Bloino, G. Zheng, J.L. Sonnenberg, M. Hada, M. Ehara, K. Toyota, R. Fukuda, J. Hasegawa, M. Ishida, T. Nakajima, Y. Honda, O. Kitao, H. Nakai, T. Vreven, J.A. Montgomery Jr., J.E. Peralta, F. Ogliaro, M. Bearpark, J.J. Heyd, E. Brothers, K.N. Kudin, V.N. Staroverov, R. Kobayashi, J. Normand, K. Raghavachari, A. Rendell, J.C. Burant, S.S. Iyengar, J. Tomasi, M. Cossi, N. Rega, J.M. Millam, M. Klene, J.E. Knox, J.B. Cross, V. Bakken, C. Adamo, J. Jaramillo, R. Gomperts, R.E. Stratmann, O. Yazyev, A.J. Austin, R. Cammi, C. Pomelli, J.W. Ochterski, R.L. Martin, K. Morokuma, V.G. Zakrzewski, G.A. Voth, P. Salvador, J.J. Dannenberg, S. Dapprich, A.D. Daniels, Ö. Farkas, J.B. Foresman, J.V. Ortiz, J. Cioslowski, D.J. Fox, Gaussian 09, Revision A.02, Gaussian, Inc., Wallingford CT, 2009.
[35] A.D. Becke, Density-functional thermochemistry III. The role of exact exchange, J. Chem. Phys. 98 (1993) 5648–5652.
[36] P.J. Stephens, F.J. Devlin, C.F. Chabalowski, M.J. Frisch, Ab initio calculation of vibrational absorption and circular dichroism spectra using density functional force fields, J. Phys. Chem. 98 (1994) 11623–11627.
[37] W.J. Hehre, R. Ditchfield, J.A. Pople, Self—consistent molecular orbital methods: XII. further extensions of Gaussian—type basis sets for use in molecular orbital studies of organic molecules, J. Chem. Phys. 56 (1972) 2257–2261.
[38] P.C. Hariharan, J.A. Pople, The influence of polarization functions on molecular orbital hydrogenation energies, Theor. Chim. Acta 28 (1973) 213–222.
[39] Y. Zhao, D.G. Truhlar, The M06 suite of density functionals for main group thermochemistry, thermochemical kinetics, noncovalent interactions, excited states, and transition elements: two new functionals and systematic testing of four M06-class functionals and 12 other functionals, Theor. Chem. Acct. 120 (2008) 215–241.
[40] R. Krishnan, J.S. Binkley, R. Seeger, J.A. Pople, Self-consistent molecular orbital methods XX. A basis set for correlated wave functions, J. Chem. Phys. 72 (1980) 650–654.
[41] M.E. Casida, C. Jamorski, K.C. Casida, D.R. Salahub, Molecular excitation energies to high-lying bound states from time-dependent density-functional response theory: characterization and correction of the time-dependent local density approximation ionization threshold, J. Chem. Phys 108 (1998) 4439–4449.
[42] M.E. Casida, Time-dependent density-functional theory for molecules and molecular solids, J. Mol. Struct. THEOCHEM 914 (2009) 3–18.
[43] R.E. Stratmann, G.E. Scuseria, M.J. Frisch, An efficient implementation of time-dependent density-functional theory for the calculation of excitation energies of large molecules, J. Chem. Phys. 109 (1998) 8218–8224.
[44] Y. Imai, K. Murata, N. Asano, Y. Nakano, K. Kawaguchi, T. Harada, T. Sato, M. Fujiki, R. Kuroda, Y. Matsubara, Selective formation and optical property of a 21-Helical columnar fluorophore composed of achiral 2-anthracenecarboxylic acid and benzylamine, Cryst. Growth Des. 8 (2008) 3376–3379.
[45] T.C. Werner, D.M. Hercules, Charge-transfer effects on the absorption and fluorescence spectra of anthroic acids, J. Phys. Chem. 74 (1970) 1030.
[46] N. DiCesare, J.R. Lakowicz, Spectral properties of fluorophores combining the boronic acid group with electron donor or withdrawing groups. Implication in the development of fluorescence probes for saccharides, J. Phys. Chem. A. 105 (2001) 6834–6840.
[47] R.S. Becker, Theory and Interpretation of Fluorescence and Phosphorescence, Wiley Interscience, New York, 1969, pp. 175–177.
[48] T.C. Werner, R. Fisch, G. Goodman, Spectral studies on aromatic esters of 9-anthroic acid, Spectroscopy Lett 7 (2006) 385–393.